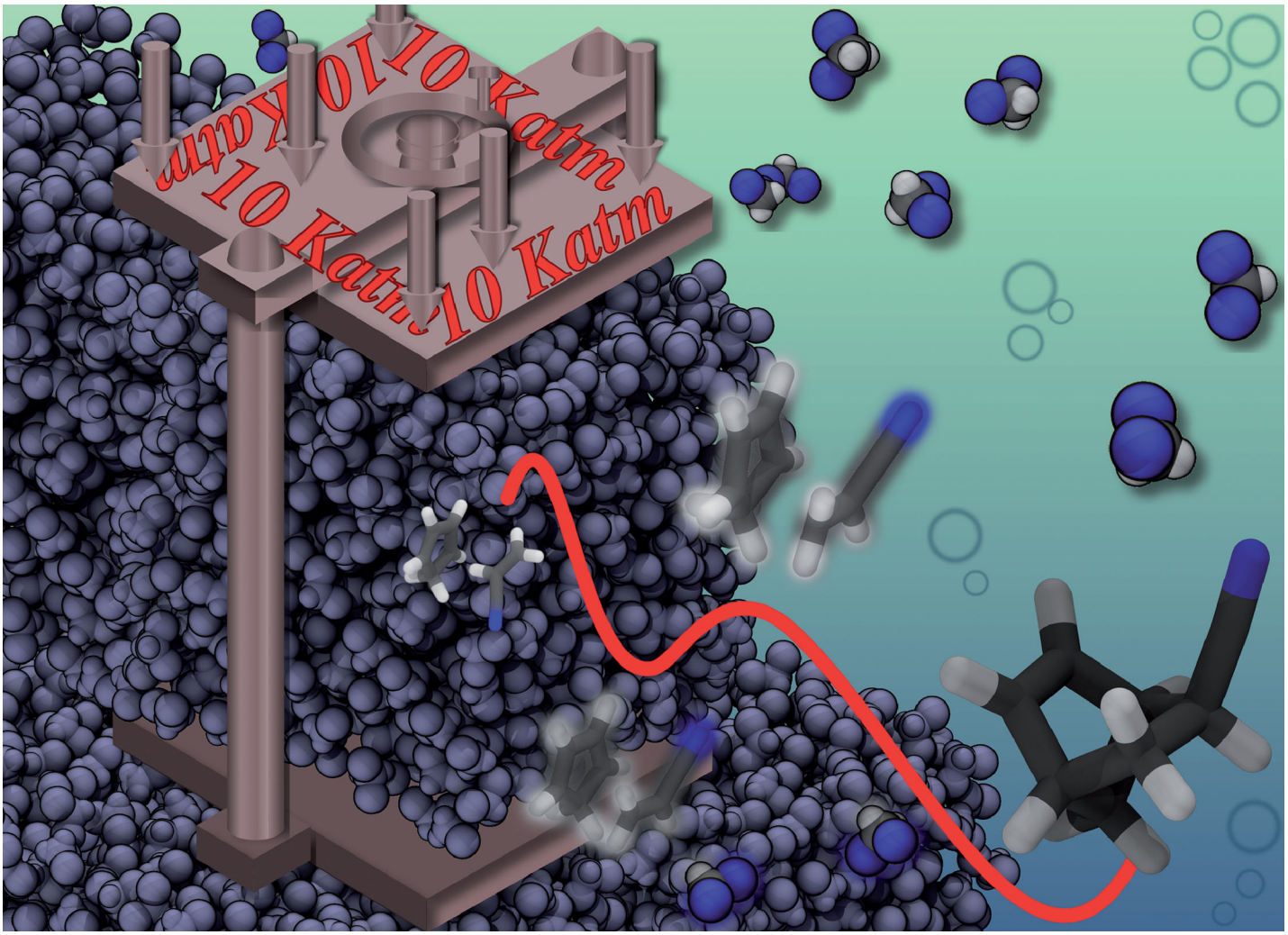

Showcasing research from D. Loco, R. Spezia, F. Cartier, I. Chataigner and J.-P. Piquemal from the Laboratoire de Chimie Théorique, Sorbonne Université, Paris, France.

Solvation effects drive the selectivity in Diels–Alder reaction under hyperbaric conditions

A multiscale modelling approach is applied to elucidate the influence of high pressure conditions on the kinetics of a Diels–Alder reaction in condensed phase. The simulations suggest a strong preference for a specific diastereomer due to solute–solvent interactions.

As featured in:

See Riccardo Spezia, Isabelle Chataigner, Jean-Philip Piquemal *et al.*, *Chem. Commun.*, 2020, **56**, 6632.

ROYAL SOCIETY OF CHEMISTRY

rsc.li/chemcomm

Registered charity number: 207890

ChemComm

ROYAL SOCIETY OF CHEMISTRY

COMMUNICATION

View Article Online
View Journal | View Issue

Cite this: *Chem. Commun.*, 2020, **56**, 6632

Received 14th March 2020,
Accepted 30th April 2020

DOI: 10.1039/d0cc01938k

rsc.li/chemcomm

Solvation effects drive the selectivity in Diels–Alder reaction under hyperbaric conditions†

Daniele Loco, [a] Riccardo Spezia,*[a] François Cartier,[a] Isabelle Chataigner *[ab] and Jean-Philip Piquemal *[ac]

High pressure effects on the Diels–Alder reaction in condensed phase are investigated by means of theoretical methods, employing advanced multiscale modeling approaches based on physically grounded models. The simulations reveal how the increase of pressure from 1 to 10 000 atm (10 katm) does not affect the stability of the reaction products, modifying the kinetics of the process by lowering considerably the transition state energy. The reaction profile at high pressure remarkably differs from that at 1 atm, showing a submerged TS and a pre-TS structure lower in energy. The different solvation between *endo* and *exo* pre-TS is revealed as the driving force pushing the reaction toward a much higher preference for the *endo* product at high pressure.

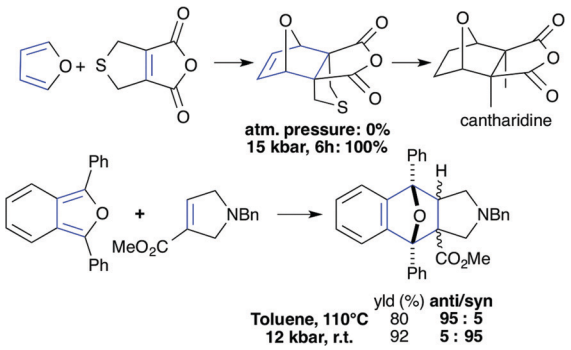

Fig. 1 Examples of successful selectivity enhancement in organic chemistry reactions.

The favourable effect of high pressure (HP) regimes on the kinetics of certain organic reactions is known for a while,[1] notably for hindered substrates. HP indeed activates reactions unfeasible under conventional conditions, often increasing chemo-, regio- and stereo-selectivities.[2–4]

HP effect has been markedly studied on the Diels–Alder cycloaddition,[5,6] a remarkable chemical transformation which still provides key solutions for the synthesis of (poly)cyclic molecules. The inertia of the components may limit its applicability, for steric or electronic reasons. The process is then usually activated by heating, using catalysts or changing solvents. Temperature increase often favors the reverse reaction, while catalysts may induce substrates and/or products degradation. Working under pressure is often an efficient alternative.

Cycloaddition reactions are characterized by very negative activation volumes ($\Delta V^{\ddagger}$ = −20 to −40 cm^3 mol^{-1})[7] and their kinetics are usually accelerated under high pressure. One of the first and most emblematic examples is the use of furan as a diene in the synthesis of cantharidin by Dauben (see Fig. 1, top).[8,9] Since then, HP activation has shown its efficiency in performing (4+2) cycloadditions involving sterically hindered[10–12] or electronically deactivated[13–16] substrates for instance. This soft and eco-compatible activation mode has thus given access to different complex and functionalized structures, in the context of total syntheses for example.[17,18] The positive influence of pressure on the diastereoselectivity of Diels–Alder cycloaddition reactions has been observed in many cases (see Fig. 1, bottom). Generally, the more compact *endo* approach is favored by a HPs.[2,19,20] In some cases *endo* kinetic adducts are obtained under hyperbaric cycloaddition, while *exo* thermodynamic ones are generated by heating.[21]

The activation observed in organic reactions in liquid phase is explained by the Evans–Polanyi equation, which connects a negative activation volume with the acceleration of the reaction with pressure increase. Based on such a theory, Ladanyi and Hynes studied pressure effects on rate constant of simple systems, finding an important dependence of the activation volume at very HP.[22]

Later, Dumas *et al.* have studied an aza-Michael addition *via* an atomistic model where the effect of pressure was included modifying the van der Waals radii.[23] More recently, Hoffmann,

[a] *Sorbonne Université, Laboratoire de Chimie Théorique, UMR 7616 CNRS, 75005 Paris, France. E-mail: riccardo.spezia@sorbonne-universite.fr*
[b] *Normandie Université, INSA Rouen, UNIROUEN, CNRS, COBRA Laboratory, F-76000 Rouen, France. E-mail: isabelle.chataigner@univ-rouen.fr*
[c] *Institut Universitaire de France, 75005, Paris, France. E-mail: jean-philip.piquemal@sorbonne-universite.fr*

† Electronic supplementary information (ESI) available. See DOI: 10.1039/d0cc01938k

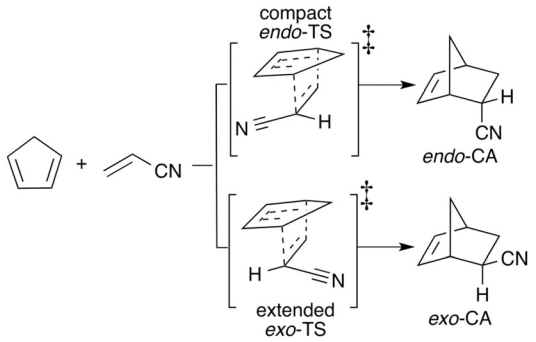

Fig. 2 Model Diels–Alder reaction used in the present work. TS: transition state, CA: cycloadduct.

Cammi and co-workers have studied the effect of pressure from a quantum chemistry approach coupled with an implicit solvation model on a set of organic reactions.[24] The activation volumes were thus evaluated from electronic densities.

To get more insight into this phenomenon, we undertook a computational modeling study of pressure effects on a prototypical Diels–Alder reaction, between cyclopentadiene and acrylonitrile (see Fig. 2).[25]

Since the HP effect can modify the solute, the solvent and their interactions, we have adopted a physically grounded description of the solvent by means of an advanced classical polarizable force field (FF),[26] coupled with a quantum chemistry method to treat the solute reacting species, which are then explicitly affected by the presence of the classical but atomistic solvent. This is what we define a polarizable variational quantum mechanics/molecular mechanics (QM/MM) method.[27–29]

To sample the large number of solute–solvent configurations needed to extract meaningful energies and properties from such atomistic models we resorted to a sequential approach: first performing full FF based molecular dynamics to have equilibrated solvent configurations at the needed temperature and high/low pressures, then including the quantum treatment of the solute in the structure sampling and performing shorter QM/MM MDs, starting from different points of the full FF-based trajectories.

The solute molecules are described within the density functional theory (DFT) approximation, with the M06-2X functional[30] and a 3-21G atomic basis set, which provides, in our benchmark reported in the ESI,† a good quality activation energy values. More details on this choice are reported in the ESI,† (Section S1). Note that it is not uncommon that a small basis set can provide results better than a larger one:[31] convergence in basis set sometimes occur only for a very large one, which would be then inadequate to perform QM/MM MDs.

During the polarizable MDs the solvent has been modeled with the AMOEBA FF, which performs correctly at different pressures without any *ad hoc* parametrization.[32] Solute was solvated by 603 CH_2Cl_2 molecules using an AMOEBA potential recently developed for organic molecules.[33] The solvent was first equilibrated at room temperature and at two different pressures (low, 1 atm and high, 10 katm) fixing the solutes in their QM optimized geometry and running about 2 ns polarizable MD simulations using the Bussi–Parrinello algorithm to keep an *NPT* ensemble.[34]

This procedure was performed for each chemical species relevant to describe the reaction pathway, which are reported in Fig. 4. Pre-transition states (pre-TS) where taken from the intrinsic reaction coordinate (IRC) which connects reactants with TS.

After an equilibration time of less than 10 ps the systems reached the equilibrium density at the two different pressures, namely 1.419(3) and 1.776(4) g mL^{-1}. These values are independent on the chemical nature of the solutes. In Fig. 3 the density time series at the beginning of the classical polarizable trajectories are reported, showing the differences between low and high pressure simulations, for which also different simulation box sizes were obtained.

Finally, the solute–solvent interaction was refined *via* a variational formulation of hybrid polarizable QM/MM, accounting for the mutual polarization between the classical and the quantum subsystems.[27–29,35] This approach was used for the first time here to investigate pressure effects on a chemical reaction.

Once the solvation was equilibrated *via* polarizable MD, QM/MM simulations were performed, either running few picoseconds QM/MM MD or single point QM/MM energy calculations (see Section S3 of ESI†), using structures sampled from the full-FF based polarizable MDs. The Tinker-HP package[36] coupled with a development version of Gaussian09 was used for all the calculations.[37]

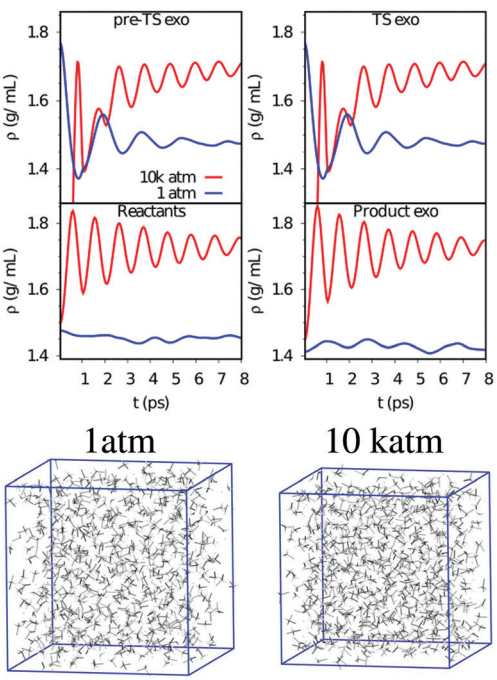

Fig. 3 (Top) Solution density's time-series along the initial part of the full-FF equilibration dynamics run for pre-TSs, TSs, cycloadducts and reactants in *exo* configuration, in CH_2Cl_2 solution. In red are reported the densities for the 10 katm MDs, while those for 1 atm MDs are in blue. Bottom) Shrinking of the MD simulation box due to the pressure increase. The cubic boxes reported are taken from two trajectories of the same solvated system at 1 and 10 katm, with a box side length of 39 and 36 Å respectively.

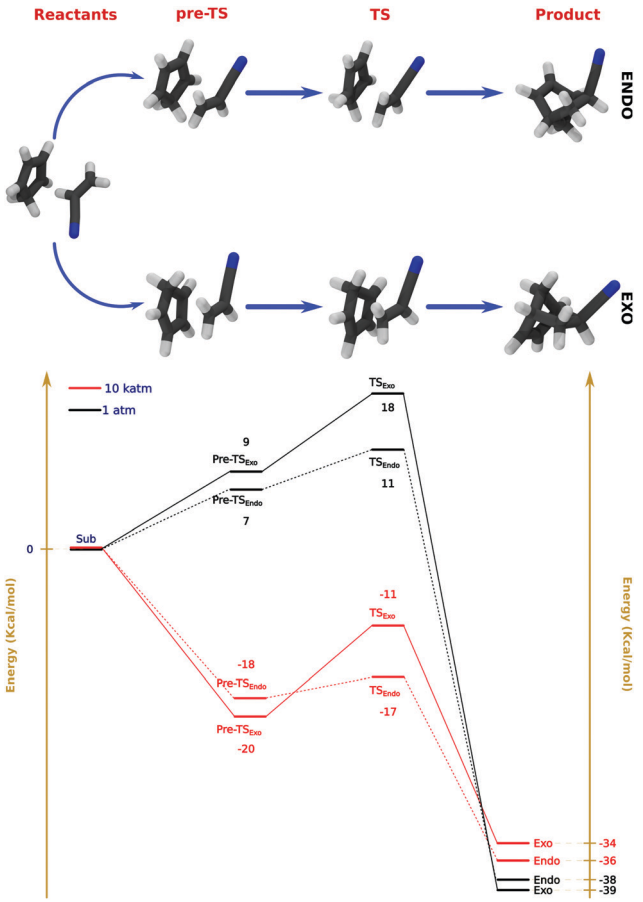

Fig. 4 (Top) Structures of the different molecular species involved in the reaction. (Bottom) Energy diagram as from QM/MM simulations, reporting the energy differences discussed in the text.

The reaction energy profiles were thus obtained extracting average energies from the simulations at different pressures, setting at zero the energy of the reactants at both 1 atm and 10 katm. Such relative energies are reported in Fig. 4.

In the 1 atm reaction pathway, the TS was found to be 11 and 18 kcal mol^{-1} higher than reactants for *endo* and *exo* approaches, respectively (with a statistical uncertainty of 1 kcal mol^{-1} for these and further energy values, as discussed in ESI†). Products were exothermic of 38 and 39 kcal mol^{-1} for *endo* and *exo* pathways. Note that for such a reaction a very small difference between the two stereomers is expected.[38] Finally, at 1 atm the pre-TS has an energy lying in between the reactants and the TS, as in the IRC calculations from which the structures were extracted.

At 10 katm the situation is very different instead: the TS was found to be energetically more stable than the reactants. Interestingly, the pre-TS structures are now more stable than the corresponding TS. However, while for the *exo* reaction, a barrier of about 9 kcal mol^{-1} was calculated between the pre-TS and the TS, for the *endo* reaction it was found to be almost zero (1 kcal mol^{-1} which lies into the uncertainty). This means that the rate constant in the case of the *endo* approach is almost under diffusion control and much faster than the *exo* one. Finally, products were similar in energy with a slight preference for the *endo* diastereomer.

Results show that the reaction is indeed kinetically favoured by a pressure increase. For the *exo* approach, an energy barrier of 18 kcal mol^{-1} at ambient pressure translates into a 9 kcal mol^{-1} one at HP; for *endo* approach, the difference is even bigger: the 11 kcal mol^{-1} barrier observed at ambient pressure almost vanishes at HP and the kinetics is then diffusion controlled. Finally, the resulting *endo* cycloadduct is favoured (due to kinetic control) with respect to *exo*, as experimentally expected.

In our microscopic description of the system, increasing the pressure triggers a compact packing of the molecules. As a consequence, the attractive interactions with the solvent molecules increase (see Table S2 of ESI† for the absolute energetics). In this respect, the use of polarizable FFs[26] is crucial: the polarization variation with the pressure ensures a large part of this. Only thanks to the fluctuations of their induced dipole, the classical solvent molecules are allowed to respond to the different pressure regimes and readjust during the compaction of the molecular packing.

On one hand, the extended *exo*-stereomers are more exposed to the solvent molecules than the compact *endo* ones. This effect is even greater in the pre-TS where the substrates are further apart: the stabilizing interactions induced by the solvent under HP show their maximum effect for the *exo* pre-TS, which is more stable than the *endo* one by 2 kcal mol^{-1}. On the other hand the TS *endo* is generally considered to be more favoured than the TS *exo*, due to the attractive secondary orbital interactions between the p orbitals that are not directly involved in the formation of the new σ bonds, according to the famous (even if still debated) proposition by Woodward and Hoffman.[39] As a net result of these two antagonistic phenomena, the *endo* TS is almost barrier less, while the *exo* one features an energy activation of 9 kcal mol^{-1}. Thus, the solvation effect explains the greater preference for the *endo* cycloadduct formation under HP.

We connect our results to the commonly accepted picture offered by the concept of activation volume. Following the approach used by Cammi and co-workers,[40] we compute molar volumes from QM/MM electron densities at the two different pressures, using them to compute activation and reaction volumes. As shown in Table 1, for each species the activation volume does not depend neither on the pressure, nor on the stereochemistry. This means that we are in the linear regime of pressure dependence, confirming experimental data.[3] Furthermore, the reaction volumes are similar, showing the high similarity between TS and products as expected for such a late transition state Diels–Alder reaction.

The pre-TS were found to be crucial in differenciating the kinetics between the *exo* and *endo* approaches at HP. This is in line with the different activation volumes calculated when the pre-TSs were considered as reactants (see Table 1). The *exo* pre-TS volume is indeed similar to the reactants one, while the *endo* pre-TS volume resembles more the corresponding TS at HP (the absolute volume of each structure is reported in Fig. S4 of ESI†).

In conclusion, we propose here that the solvation plays a fundamental role on the pressure effect on this Diels–Alder

Table 1 Activation volume $\Delta V^{\ddagger}$ and reaction volume ΔV^{react} for the reaction under investigation computed from the SCF QM/MM electron density with Monte-Carlo integration by Gaussian 09.[37,40] The values, with associated 95% confidence interval, are reported in cm^3 mol^{-1}. The molecular volume is defined as the volume inside a contour ρ (electron per $Bohr^3$) density set at the Gaussian09 default value

	$\Delta V^{\ddagger}$		ΔV^{react}	
	Endo	*Exo*	*Endo*	*Exo*
1 atm	-8.65 ± 2.60	-10.09 ± 3.60	-10.76 ± 0.60	-10.24 ± 0.60
10 katm	-9.00 ± 3.20	-8.94 ± 3.60	-11.12 ± 0.60	-10.594 ± 0.60

	$\Delta V_{pre\text{-}TS}$	
	Endo	*Exo*
1 atm	-6.34 ± 4.10	-3.71 ± 4.80
10 katm	-4.40 ± 4.10	-7.40 ± 4.80

prototypical cycloaddition. Under HP, the efficient solvation of the TSs lowers the energy barriers and explain the acceleration of the process. In addition to this phenomenon, the *exo* pre-TS arrangement, more exposed to solvent molecules, is favorably solvated under HP and more stabilized than the *endo* one, making the passage to the corresponding TS more challenging. In the meantime, the compact *endo* TS remains favored thanks to its attractive secondary orbital interactions. These two parallel phenomena explain the enhancement of the diastereoselectivity and the greater *endo* preference for Diels–Alder cycloaddition under HP. Note that this interpretation is somehow in line with the work by Houk and Bickelhaupt, showing that a distortion/interaction model is especially fruitful for explaining cycloaddition reactivity.[41] The QM/MM method developed in our group shows how pressure effects in the condensed phase can be modeled for an archetypal Diels–Alder reaction. The original approach proposed will certainly find other applications, not only for transformations under HP, but also to further investigate the crucial role of solvents/additives in organic reactions.

Conflicts of interest

There are no conflicts to declare.

Notes and references

1 W. C. Röntgen, *Ann. Phys. Chem.*, 1892, **281**, 98–107.
2 W. J. le Noble and H. Kelm, *Angew. Chem., Int. Ed. Engl.*, 1980, **19**, 841–856.
3 R. van Eldik and F. Klärner, *High Pressure Chemistry: Synthetic, Mechanistic, and Supercritical Applications*, Wiley, 2002.
4 I. Chataigner and J. Maddaluno, in *Activation methods: Sonochemistry and High Pressure*, ed. C. J. Goddard, and M. Malacria, Wiley, 2019, pp. 95–149.
5 K. Matsumoto and A. Sera, *Synthesis*, 1985, 999–1027.
6 K. Matsumoto, H. Hamana and H. Iida, *Helv. Chim. Acta*, 2005, **88**, 2033–2234.
7 A. Drljaca, C. D. Hubbard, R. van Eldik, T. Asano, M. V. Basilevsky and W. J. le Noble, *Chem. Rev.*, 1998, **98**, 2167–2290.
8 W. G. Dauben, C. R. Kessel and K. H. Takemura, *J. Am. Chem. Soc.*, 1980, **102**, 6893–6894.
9 C. Petrier and J. L. Luche, *J. Org. Chem.*, 1985, **50**, 910–912.
10 B. Gacem and G. Jenner, *J. Phys. Org. Chem.*, 2004, **17**, 221–225.
11 G. Jenner, *Tetrahedron*, 2005, **61**, 3621–3635.
12 R. Baker, D. L. Selwood, C. J. Swain, N. M. H. Webster and J. Hirshfield, *J. Chem. Soc., Perkin Trans. 1*, 1988, 471–480.
13 R. W. Aben, J. Keijsers, B. Hams, C. G. Kruse and H. W. Scheeren, *Tetrahedron Lett.*, 1994, **35**, 1299–1300.
14 K. Kumamoto, I. Fukada and H. Kotsuki, *Angew. Chem., Int. Ed.*, 2004, **43**, 2015–2017.
15 A. Chrétien, I. Chataigner and S. R. Piettre, *Chem. Commun.*, 2005, 1351–1353.
16 N. Chopin, H. Gérard, I. Chataigner and S. R. Piettre, *J. Org. Chem.*, 2009, **74**, 1237–1246.
17 C. L. Hugelshofer and T. Magauer, *Synthesis*, 2014, 1279–1296.
18 M. Uroos, P. Pitt, L. M. Harwood, W. Lewis, A. J. Blake and C. J. Hayes, *Org. Biomol. Chem.*, 2017, **15**, 8523–8528.
19 M. Buback, J. Abeln, T. Hübsch, C. Ott and L. F. Tietze, *Liebigs Ann.*, 1995, 9–11.
20 L. F. Tietze, M. Henrich, A. Niklaus and M. Buback, *Chem. – Eur. J.*, 1999, **5**, 297–304.
21 N. Pichon, A. Harrison-Marchand, P. Mailliet and J. Maddaluno, *J. Org. Chem.*, 2004, **69**, 7220–7227.
22 B. M. Ladanyi and J. T. Hynes, *J. Am. Chem. Soc.*, 1986, **108**, 585–593.
23 F. Dumas, C. Fressigné, J. Langlet and C. Giessner-Prettre, *J. Org. Chem.*, 1999, **64**, 4725–4732.
24 B. Chen, R. Hoffmann and R. Cammi, *Angew. Chem., Int. Ed.*, 2017, **56**, 11126–11142.
25 K. Nakagawa, Y. Ishii and M. Ogawa, *Tetrahedron*, 1976, **32**, 1427–1429.
26 J. Melcr and J.-P. Piquemal, *Front. Biosci.*, 2019, **6**, 143.
27 D. Loco, E. Polack, S. Caprasecca, L. Lagardère, F. Lipparini, J.-P. Piquemal and B. Mennucci, *J. Chem. Theory Comput.*, 2016, **12**, 3654–3661.
28 D. Loco, L. Lagardère, S. Caprasecca, F. Lipparini, B. Mennucci and J.-P. Piquemal, *J. Chem. Theory Comput.*, 2017, **13**, 4025–4033.
29 D. Loco, L. Lagardère, G. A. Cisneros, G. Scalmani, M. Frisch, F. Lipparini, B. Mennucci and J.-P. Piquemal, *Chem. Sci.*, 2019, **10**, 7200–7211.
30 Y. Zhao and D. G. Truhlar, *Theor. Chem. Acc.*, 2008, **120**, 215–241.
31 A. Martin-Somer, M.-P. Gaigeot, M. Yanez and R. Spezia, *Phys. Chem. Chem. Phys.*, 2014, **16**, 14813–14825.
32 P. Ren and J. W. Ponder, *J. Phys. Chem. B*, 2004, **108**, 13427–13437.
33 X. Mu, Q. Wang, L.-P. Wang, S. D. Fried, J.-P. Piquemal, K. N. Dalby and P. Ren, *J. Phys. Chem. B*, 2014, **118**, 6456–6465.
34 G. Bussi, D. Donadio and M. Parrinello, *J. Chem. Phys.*, 2007, **126**, 014101.
35 F. Lipparini, *J. Chem. Theory Comput.*, 2019, **15**, 4312–4317.
36 L. Lagardère, L.-H. Jolly, F. Lipparini, F. Aviat, B. Stamm, Z. F. Jing, M. Harger, H. Torabifard, G. A. Cisneros, M. J. Schnieders, N. Gresh, Y. Maday, P. Y. Ren, J. W. Ponder and J.-P. Piquemal, *Chem. Sci.*, 2018, **9**, 956–972.
37 M. J. Frisch, *et al.*, *Gaussian Development Version, Revision H.36*, Gaussian Inc., Wallingford CT, 2010.
38 O. Larranaga and A. de Cozar, *ChemistryOpen*, 2019, **8**, 49–57.
39 C. S. Wannere, A. Paul, R. Herges, K. N. Houk, H. F. Schaefer III and P. Von Ragué Schleyer, *J. Comput. Chem.*, 2007, **28**, 344–361.
40 T. Yang, R. Fukuda, R. Cammi and M. Ehara, *J. Phys. Chem. A*, 2017, **121**, 4363–4371.
41 F. M. Bickelhaupt and K. N. Houk, *Angew. Chem., Int. Ed.*, 2017, **56**, 10070–10086.